18

A Lattice Gas Approach to the Mexico City Wind Field Estimation Problem

Alejandro Salcido and Ana Teresa Celada Murillo
Instituto de Investigaciones Eléctricas, División de Energías Alternas
México

1. Introduction

Although in 1992 the United Nations Environment Programme and the World Health Organization included Mexico City among the megacities with the worst air pollution problems (UNEP & WHO, 1992), the environmental actions carried out by the local governments of the Mexico City Metropolitan Area (MCMA) in the following fifteen years, particularly in the period 2000-2006, produced very important reductions in the emissions of air pollutants. Emission reductions around 86% in sulphur dioxide (SO_2), 60% in carbon monoxide (CO), 30% in nitrogen oxides (NO_x), 50% in PM_{10} (particulate matter < 10 μm in diameter), and 40% in volatile organic compounds (VOC), were reported for the years 1990-2006 in the official emission inventory (SMA-GDF, 2008). Nevertheless, nowadays, close to 1.8 megatons of CO, 187 kilotons of NOx, 6 kilotons of SO_2, 21 kilotons of PM_{10}, and 512 kilotons of VOC are still being produced in the MCMA and released to its ambient atmosphere every year (SMA-GDF, 2008). The critical air pollutants in MCMA are ozone (O_3), PM_{10} and $PM_{2.5}$ with concentrations above their daily and annual US air quality standards (Bravo & Torres, 2002). Ozone, however, is by far the most important air pollutant because of the frequency of occurrence of high levels, persistence, and spatial distribution (Bravo & Torres, 2002; Bonner et al., 1998; Osornio-Vargas et al., 2006).

Besides the emissions, however, other very important factors, such as the geographical setting, the topography, the meteorology, and the properties of the urban surface, and their possible interactions, must be taken into account in the analyses to understand properly the complexity and gravity of the MCMA air pollution problem. The MCMA is situated inside a subtropical basin (19.0-20.0 °N, 98.5-99.5 °W) which extends over an area of 60 x 60 km², approximately, and has an average altitude of 2240 m. As it is shown in Figure 1, the MCMA is surrounded by high mountains on three sides: west, south and east. To the west and south are the *Sierra Las Cruces* and the *Sierra Ajusco-Chichinautzin* (which its highest point is the peak *Cruz del Marques* in the volcano *Ajusco*, with an altitude of 3937 m). To the east, starting with the *Sierra Santa Catarina*, there is a north-south barrier consisting of three peaks, with the volcanoes *Iztaccihuatl* and *Popocatepetl* reaching elevations of 5222 and 5465 meters above sea level (masl), respectively. At the southeast corner of the MCMA basin the terrain falls, creating a low-lying gap through the mountains. To the north, the basin extends into the Mexican plateau and the arid interior of the country, with the *Sierra de Guadalupe* creating a

small 800 m barrier above the basin floor. Its climate, otherwise, is usually classified into two seasons: the rainy season from May to October, and the dry season from November to April. This classification stems from the two main meteorological patterns on the synoptic scale: dry westerly winds with anticyclonic conditions from November until April, and moist flows from the East due to the weaker trade winds along the other six months. Very often, however, the meteorology at the MCMA is more complex than this simple classification. Important interactions of the basin with the Mexican plateau and the lower coastal areas may occur. Moreover, due to the MCMA location, large-scale pressure gradients are generally weak, and a very strong solar radiation is registered there throughout the year. In 2001, the MCMA global solar radiation ranged 150-300 W/m² in average, with maximum values from 800 to 1100 W/m²; and wind speeds from 2 to 3 m/s were observed at urban sites, and from 3 to 4 m/s in suburban areas, in average (Salcido et al, 2003a). These conditions, combined with the surrounding mountains, are ideal for the development of thermally driven winds, including upslope, downslope, and heat island winds.

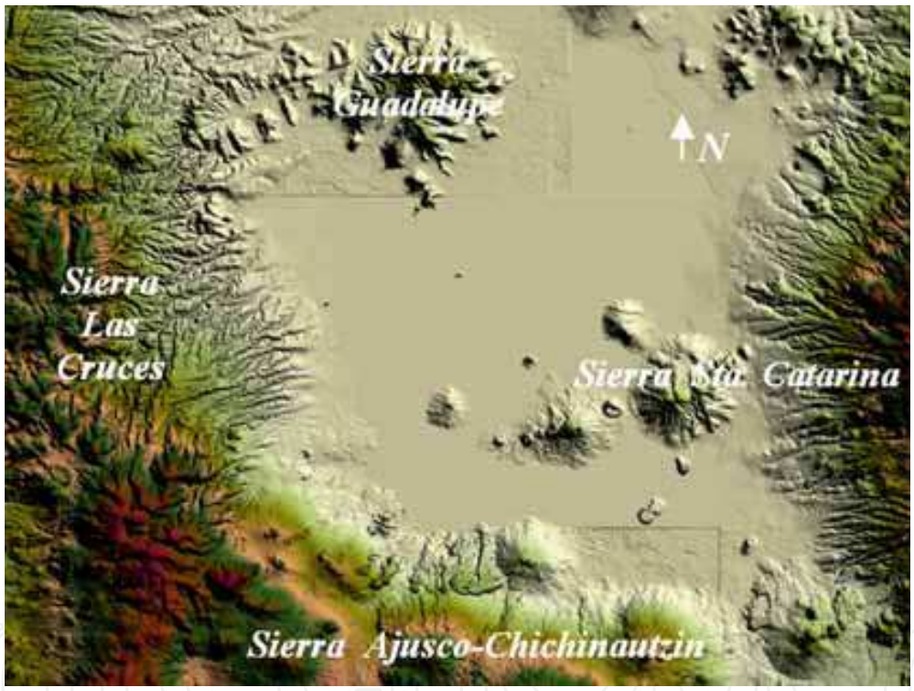

Fig. 1. Main topographic features of the Mexico City Metropolitan Area

The knowledge of the wind circulation events and their possible organization in patterns constitute an important issue to understand how the emissions of air pollutants may be dispersed in an urban settlement and how its air pollution may be exported towards the neighboring sites. Although the MCMA is surrounded by high mountains and it may lead to the trapping of air pollution up to for several days, it is also frequent that the mixing height may reach values higher than 2600 m above ground level (Salcido et al, 2003b), and these conditions favor exportation of air pollution from the MCMA to its surroundings (Castro & Salcido, 2006). On another hand, because the changes in the urban design and the spatial distribution of the built can affect the surface wind circulation in the cities, the short

and long term evolution of the urban wind patterns are relevant also for urban bioclimatic studies. Nowadays, this is also a particularly important issue in relation with the MCMA air pollution problem because in the last seven years the urban morphology was changed significantly by the construction of a second traffic floor above the Periferico freeway (a primary via which surrounds the city from north to south) and by an explosive growing of the number of the skyscrapers and other big buildings in the city. These all are wind field applications that belong to the meso-γ scale or turbulence scale meteorology problems.

The theoretical basis of meteorology is in the Navier –Stokes equations, which constitute a system of coupled and non-linear partial differential equations. For small velocities, these equations can be linearised and solved without much difficulty, analytically if the solid boundaries involved are simple, and numerically otherwise. However, when air flow velocities are large, instabilities may appear and exact analytical methods can no longer be used. Even numerical methods are difficult to use, chiefly because scales of different sizes must be taken into account, which forces grids either to be very small or variable.

In practice, a lot of powerful computer simulation tools for diagnostic and prognostic purposes, ordinarily known as meteorological models, have been developed (and still are being developed) to find out the wind fields and other meteorological variables for a variety of applications. A diagnostic model simply provides an estimate of a steady state condition because it contains no time-tendency terms, includes little physics in its calculations and provides meteorological fields derived by appropriate interpolation and extrapolation of available data. A prognostic model, instead, does incorporate meteorology physics and can be used to forecast the space-time evolution of the system by numerical integration of time-dependent differential equations. However, the numerical solutions depend strongly on boundary conditions and initial values; so that special care must be taken to correctly initialise all meteorological variables in the computational domain and to correctly define the time-varying physics at the boundaries. Two excellent prognostic meteorological models are the PSU/NCAR mesoscale model (known as MM5) and the Weather Research and Forecasting (WRF) model. These two models are complex and heavy numerical simulation instruments adequate only for mesoscale meteorology problems (MM5, 2003).

A quite different strategy to simulate fluid behaviour has been developed in the last two decades using the cellular automata techniques introduced by John von Neumann and Stanislaw Ulam in the early 1950s (von Neumann, 1966). Fully discrete models obeying cellular automata rules have been developed for the microscopic motion of the particles of a gas, such that the coarse-grained behaviour (in the thermodynamic limit) lies in the same universality class as the fluid flow phenomenon. This class of dynamical systems, known as lattice gas models, consist of a regular lattice, each site of which can have a finite number of states representing the directions of motion of the gas particles, and evolves in discrete time steps obeying a set of homogeneous local rules which define the system dynamics. These rules must be defined in such a way that the physical laws of conservation of mass, momentum and energy are fulfilled during the propagation and collisions of the gas particles (Boghosian, 1999). Typically, only the nearest neighbours are involved in the updating of any lattice site.

The first attempt along these lines was undertaken by Leo P. Kadanoff and Jack Swift in 1968 (Kadanoff & Swift, 1968). The Kadanoff-Swift model exhibits many features of real fluids, such as sound-wave propagation, and long-time tails in velocity autocorrelation functions. As the authors noted, however, it does not faithfully reproduce the correct motion

of a viscous fluid (Boghosian, 1999). The next advance in the lattice modelling of fluids came in the mid 1970's, when J. Hardy, O. de Pazzis and Y. Pomeau introduced a new lattice model (the HPP model, named for its authors) with a number of innovations that warrant discussion here (Hardy et al, 1973; Hardy et al., 1976). Like the Kadanoff-Swift model, the HPP model gives rise to anisotropic hydrodynamic equations that are not invariant under a global spatial rotation. At the time, this was not considered a problem, since the real purpose of these models was to study the statistical physics of fluids, and both models could do this well. Traditional computational fluid dynamicists, however, were not inclined to take notice of this as a serious numerical method unless and until a way was found to remove the unphysical anisotropy (Boghosian, 1999). Thirteen years passed from the introduction of the HPP model to the solution of the anisotropy problem in 1986 by Uriel Frisch, Brosl Hasslacher and Yves Pomeau (Frish et al, 1986), and simultaneously by Stephen Wolfram (Wolfram, 1986). Frisch, Hasslacher and Pomeau demonstrated that it is possible to simulate the Navier-Stokes equations of fluid flows by using a cellular automaton of gas particles on a hexagonal lattice, with extremely simple translation and collision rules governing the movement of the particles. In the FHP model, named after the authors of the first reference given above, all the particles have unit mass and move with the same speed hopping from site to site in a hexagonal two-dimensional lattice. The dynamics of this system involves a set of collision rules such that momentum and particle number are conserved (kinetic energy is trivially conserved). From a strict theoretical point of view, it is not clear at the present time if the lattice gas collective equations are equivalent to the Navier-Stokes equations, or if they include them as a particular case. However, there has been a growing interest in studying the viscous fluid flow using lattice gas models due to its great facility to handle complex boundary and initial conditions, and also because the computer simulations have shown that lattice gases behave like normal fluids under some restricted conditions (Hasslacher, 1987; Salcido & Rechtman, 1991, 1993; Rechtman & Salcido, 1996; Salcido, 1993, 1994). The FHP model, in particular, is now considered as an efficient way to simulate viscous flows at moderate Mach numbers in situations involving complex boundaries. However, it is unable to represent thermal or diffusional effects since all particles have the same speed and are of the same nature (Chen et al., 1989). Maybe the simplest lattice gas with thermal properties is a nine-velocities model defined on a square two-dimensional lattice where particles may be at rest or travelling to their nearest or next nearest neighbours (Chen et al., 1989; Rechtman et al., 1990, 1992; Salcido & Rechtman, 1991, 1993; Rechtman & Salcido, 1996).

One of the first attempts to use a lattice gas as an alternative approach in air pollution modelling applications can be found in the work by A. Salcido (Salcido, 1993, 1994; Salcido et al., 1993). There, it is shown how the lattice gas rules, in spite of their relative simplicity, are sufficient to simulate, at least qualitatively, some complex processes affecting unsteady dispersion, including momentum exchange with the surrounding atmosphere and deposition. More recent attempts are found in the work by A. Sciarretta and R. Cipollone (Sciarretta & Cipollone, 2001, 2002; Sciarretta 2006), where a comprehensive stochastic lattice gas model, which provides also reliable quantitative predictions, is presented.

In this work we describe and apply a two-dimensional (2D) lattice gas approach to estimate the MCMA surface wind field from the hourly meteorological data registered at the stations of the official atmospheric monitoring network. This approach is based on the simplest lattice gas with thermal properties. It is a square lattice gas model with interactions up to

second nearest neighbours that conserve the number of particles, momentum and kinetic energy. Within this framework, the best wind field estimate is given by the steady state lattice gas flow which is consistent with the wind velocity values imposed to a number of control lattice sites representing the positions of the meteorological stations, and with a number of forbidden lattice sites that represent the solid boundaries defined by the MCMA topography. The application to the MCMA study case was carried out for the meteorological conditions which prevailed there during the 1994 summertime. As a first step, a model wind direction state, which reflects in a discrete and simplified way the main features of the complex spatial structure of the surface wind circulation events, is used to obtain the density of states of wind direction of the MCMA, as well as a qualitative and quantitative identification of the main wind circulation patterns for daytime and nighttime hours of the dry and rainy seasons of 1994. This first analysis phase helped us to select the particular (but important) daytime and nighttime MCMA wind circulation events which we considered as study cases for the lattice gas simulation of the respective wind fields. The computer simulations were carried out using wind velocity data obtained during a four-site micrometeorological campaign we carried out in Mexico City during the 1994 summertime. The results were compared against the wind data registered by the stations of the official atmospheric monitoring network of Mexico City. A previous description of these results was reported by A. Salcido, A. T. Celada and T. Castro in 2008 (Salcido et al., 2008).
The rest of this chapter is organized as follows: Section 2 is dedicated to describe the basis of the nine-velocity lattice gas model, its equilibrium theory, and some of the simulations we have carried out to test the hydrodynamic behavior of this model. In Section 3, the lattice gas approach we are proposing for the wind field estimation problem is detailed. In Section 4, the characterization of the MCMA wind circulation events that prevailed there in 1994 is presented in terms of the density of states of wind direction and the main wind circulation patterns that can be identified by means of parameters such as the mean wind direction, the vorticity and the divergence of the MCMA wind direction states. In Section 5, it is described and discussed the application of the lattice gas model in estimating the MCMA wind field for some particular wind circulation events which occurred at both daytime and nighttime hours of the 1994 summertime, as well as the comparison of the simulation results against wind velocity data registered at the stations of the official atmospheric network of Mexico City. Finally, it is included a section devoted to conclusions and suggestions for future work.

2. The Nine-Velocity Lattice Gas Model

We will consider a cellular automaton defined on a square 2D lattice containing N_X times N_Y sites. The state at any lattice site **r** indicates the presence or absence of particles travelling in nine allowed directions defined by the vectors:

$$\mathbf{e}_\alpha = \begin{cases} 0 & \alpha = 0 \\ \cos((\alpha-1)\frac{\pi}{4})\mathbf{u}_1 + \sin((\alpha-1)\frac{\pi}{4})\mathbf{u}_2 & \alpha = 1,...,8 \end{cases} \quad (1)$$

where $\mathbf{u}_1$ and $\mathbf{u}_2$ are unit vectors along the positive directions of X and Y axes, respectively. The time step and the lattice step along the axes are both defined as unit. The allowed particle speeds c_α and kinetic energies ε_α (assuming particles of unit mass) are defined by

$$c_\alpha = \begin{cases} 0 & \alpha = 0 \\ 1 & \alpha = 1,3,5,7 \\ \sqrt{2} & \alpha = 2,4,6,8 \end{cases} \tag{2}$$

$$\varepsilon_\alpha = \frac{c_\alpha^2}{2} = \begin{cases} 0 & \alpha = 0 \\ \frac{1}{2} & \alpha = 1,3,5,7 \\ 1 & \alpha = 2,4,6,8 \end{cases} \tag{3}$$

This means that the model only takes into account particle interactions to the nearest and the next nearest neighbours. An exclusion principle is obeyed by the lattice gas particles in the sense that at any site **r** and at any time *t* there can be no more than one particle moving in each of the allowed directions $\mathbf{e}_\alpha$. This exclusion principle has deep consequences on the collective (or macroscopic) behaviour of the model.

The state $S(\mathbf{r},t)$ at any lattice site **r** at any time *t* is given by a set of nine Boolean fields, $S_\alpha(\mathbf{r},t)$. Each one of these field variables takes the value 1 (0) in the presence (absence) of a particle traveling in direction α at site **r** and time *t*. The time evolution of the model is defined by a set of, at least, three homogeneous local operators, **T**, **C** and **B**, that represent the translation of particles, the collision between particles, and the collision of particles against fixed obstacles or solid boundaries, respectively. Formally, this can be expressed as

$$S(\mathbf{r},t+1) = \mathbf{B} \circ \mathbf{C} \circ \mathbf{T}\left(\left\{ S(\mathbf{r}',t) \middle| \mathbf{r}' \in V_r \right\}\right) \tag{4}$$

where V_r denotes the neighborhood of site **r** that contains the site itself, and its nearest and next nearest neighbors. As it is illustrated in Figure 2, the translation operator **T** explores all the sites in the neighborhood and moves the particles pointing towards the central site to it. These particles form the input state for the collision operator **C** and the output is some other state that has the same number of particles, momentum and energy. The nontrivial collisions of two and three particles are shown schematically in Figure 3 where an open circle indicates a particle at rest and each entry represents all its possible rotations. For each entry, any state may be chosen as the input of the collision and the remaining states are the possible outputs. Although Figure 3 shows only the nontrivial two and three particle collisions, the evolution of the automaton takes into account all particle collisions that can occur involving up to 9 particles. The translation and collision operators define the lattice gas microdynamics and are applied synchronously to all the sites of the lattice. The obstacle operator takes into account boundary conditions and the presence of obstacles. A particle that collides with an obstacle may invert its direction (to simulate, on the collective level, a no-slip condition) or may be reflected (to simulate now a slip condition). Other operators can be introduced to simulate effects due to heating or gravitational forcing (Rechtman et al., 1990; Salcido & Rechtman, 1991). The heating operator, for example, attempts to simulate a heat exchange between the system and its surroundings in such a way that the average energy of the system assumes a given value. A simple implementation of the heating operator is as follows. After the action of the translation, collision and obstacle operators a

small percentage of sites is chosen at random, the average energy is calculated and compared with a given energy control value. If the average energy takes a value greater (smaller) than the control energy, a new state is assigned to each of the chosen sites that has the same number of particles but smaller (greater) energy.

In spite of the simplicity of the rules that define the microdynamics of this model, the computer simulations show that at the collective level it behaves very similar to a real gas under certain conditions, but also can have a non classical behavior under other conditions. In the next two subsections, we present first the equilibrium theory of the 9-velocity lattice gas model and later some few computer simulations we carried out to test its hydrodynamic behavior, both qualitatively and quantitatively.

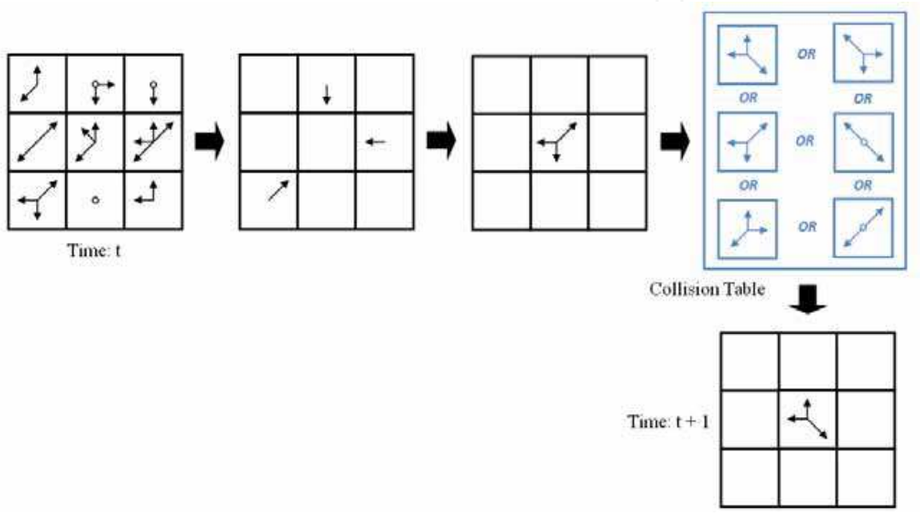

Fig. 2. The propagation and collision of the lattice gas particles.

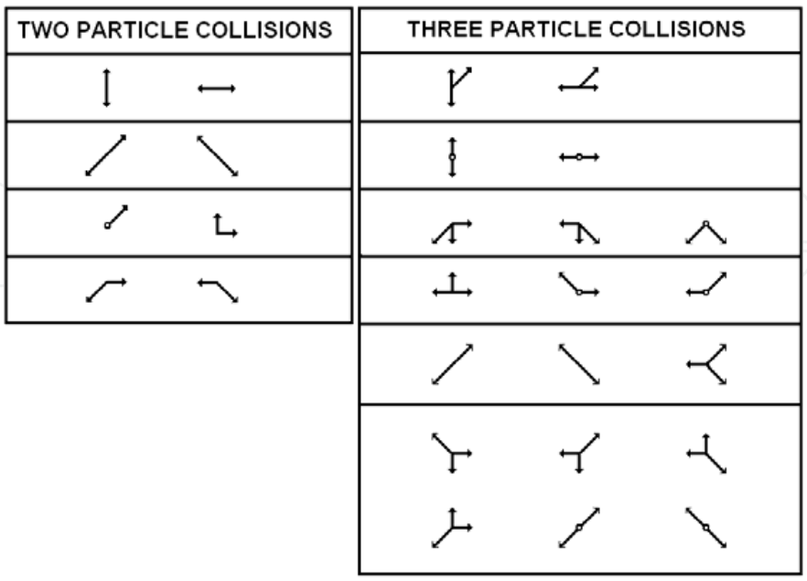

Fig. 3. Collisions involving two and three particles.

2.1 Equilibrium Properties

Let n, e and n_α denote the average number of particles per site, the average energy per site, and the average number of particles per site moving in direction $\mathbf{e}_\alpha$ at site $\mathbf{r}$ and at time t, respectively. Then

$$n = \sum_\alpha n_\alpha \tag{5}$$

$$e = \sum_\alpha n_\alpha \varepsilon_\alpha \tag{6}$$

Due to the exclusion principle there are a lower bound ($e_{\min}$) and an upper bound ($e_{\max}$) on the energy per site e which depend on the average number of particles per site n as follows:

$$e_{\min} = \begin{cases} 0 & 0 \le n < 1 \\ \dfrac{n-1}{2} & 1 \le n < 5 \\ n-3 & 5 \le n \le 9 \end{cases} \tag{7}$$

$$e_{\max} = \begin{cases} n & 0 \le n < 4 \\ \dfrac{n+4}{2} & 4 \le n < 8 \\ 6 & 8 \le n \le 9 \end{cases} \tag{8}$$

The graphs of these functions are shown in Figure 4. The area between the two curves represents the set of the allowed states (n, e) of the model.

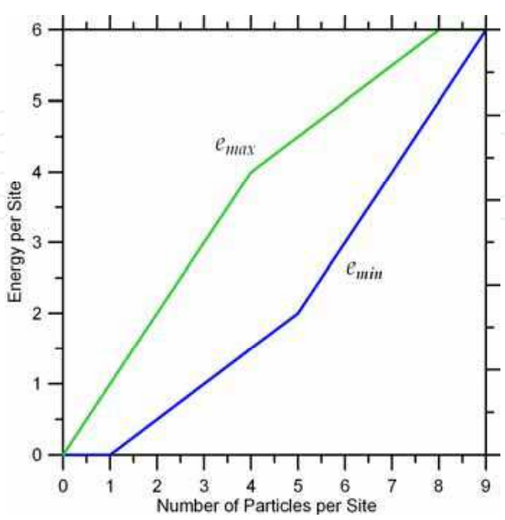

Fig. 4. Minimum and maximum allowed energies.

Now, following the microcanonical equilibrium statistical mechanics, the equilibrium thermodynamic properties can be obtained from the distribution densities $\tilde{n}_\alpha$ that maximize the entropy per site of the system (Salcido & Rechman, 1991)

$$s = -k\sum_{\alpha}\left[n_\alpha \ln n_\alpha + (1-n_\alpha)\ln(1-n_\alpha)\right] \tag{9}$$

under the constraints imposed by the equations (5) and (6). In this equation k is the Boltzmann constant, which hereafter will be considered equal to 1, for simplicity. By employing the method of undetermined Lagrange multipliers, the distribution densities $\tilde{n}_\alpha$ of the equilibrium states are obtained:

$$\tilde{n}_\alpha = \frac{1}{1+e^{(a+b\varepsilon_\alpha)}} \tag{10}$$

where a and b are the Lagrange multipliers. Now, to get some insight about the physical meaning of the Lagrange multipliers a and b, we note that, using equations (10), the entropy can be written as

$$s = an + be - \sum_{\alpha}\ln(1-\tilde{n}_\alpha) \tag{11}$$

Then, a formal comparison of this equation with the well known Euler equation of thermodynamics for a gas of particles,

$$s = -\frac{\mu}{T}n + \frac{1}{T}e + \frac{P}{T} \tag{12}$$

suggests the following thermodynamic-like interpretation:

$$\begin{aligned} a &= -\frac{\mu}{T} \\ b &= \frac{1}{T} \\ \frac{P}{T} &= -\sum_{\alpha}\ln(1-\tilde{n}_\alpha) \end{aligned} \tag{13}$$

In the Euler equation (12), s is the entropy per unit volume, n is the density of the number of particles, T is the temperature, μ is the chemical potential, e is the internal energy per unit volume, and P is the pressure.

Strictly speaking, the first two equations (13) just define the new parameters T and μ in terms of the Lagrange multipliers a and b, and the last one defines P. However, the use of these properties, which we will call temperature (T), chemical potential (μ), and pressure (P)

of the lattice gas, opens a useful framework for the physical analysis and interpretation of lattice gas behavior. In terms of the temperature and chemical potential, the distribution densities $\tilde{n}_\alpha$ of the equilibrium states can be expressed as

$$\tilde{n}_\alpha = \frac{1}{1 + e^{(\varepsilon_\alpha - \mu)/T}} \tag{14}$$

So, at equilibrium the lattice gas particles will organize themselves among the possible velocities according to a Fermi-Dirac distribution. This is a consequence of the exclusion principle that must be obeyed by the lattice gas particles. Under equilibrium conditions, as it is implied also by equation (14), the same number of particles moves along each diagonal direction and also along the vertical and horizontal ones:

$$\tilde{n}_1 = \tilde{n}_3 = \tilde{n}_5 = \tilde{n}_7 \qquad \tilde{n}_2 = \tilde{n}_4 = \tilde{n}_6 = \tilde{n}_8 \tag{15}$$

These theoretical results agree with the computer simulations we performed to test the equilibrium properties of the model. We started with a 200 x 100 sites lattice and particles tossed at random in position and direction of motion keeping the average number of particles per site n fixed. With a heating operator, the lattice gas was cooled or heated for 500 time steps to fix its energy to a given control value and then left to equilibrate for another 500 time steps. Finally the experimental distributions densities were computed. In Figure 5, the plots for the theoretical equilibrium distribution densities $\tilde{n}_0$, $\tilde{n}_1$, and $\tilde{n}_2$, including the corresponding simulation results, are presented for $n = 1$ and $n = 3$. This figure shows also that a population inversion takes place in the high energy limit.

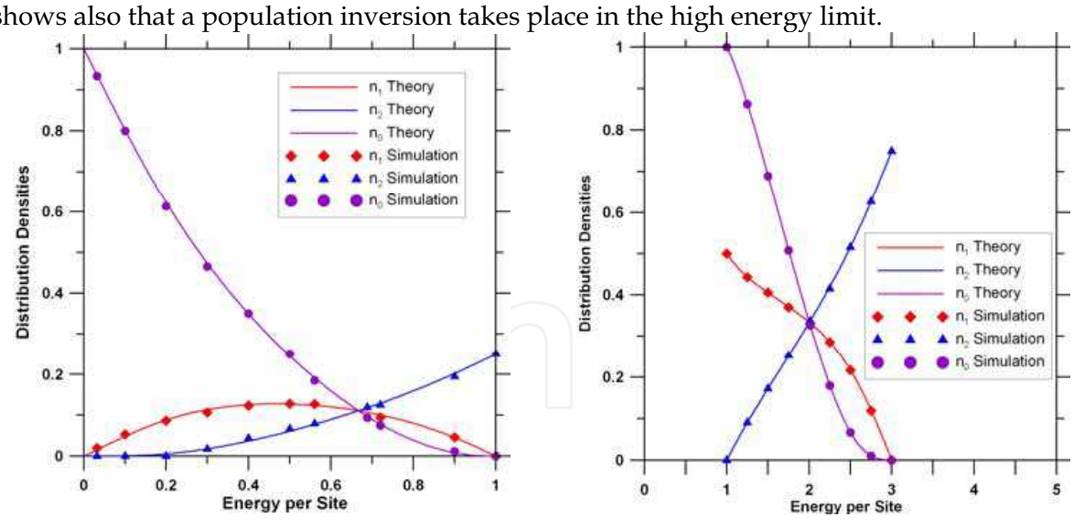

$n = 1$ $n = 3$

Fig. 5. Comparison of the theoretical and experimental (simulated) equilibrium distribution densities for average numbers of particles $n = 1$ ($e_{min} = 0$ and $e_{max} = 1$) and $n = 3$ ($e_{min} = 1$ and $e_{max} = 3$).

In figures 6, the plots for the entropy per site (Fig. 6a), the temperature (Fig. 6b), the pressure (Fig. 6c), and the chemical potential (Fig. 6d), as functions of the energy per site e, for a number of particles per site $n = 1$, are presented.

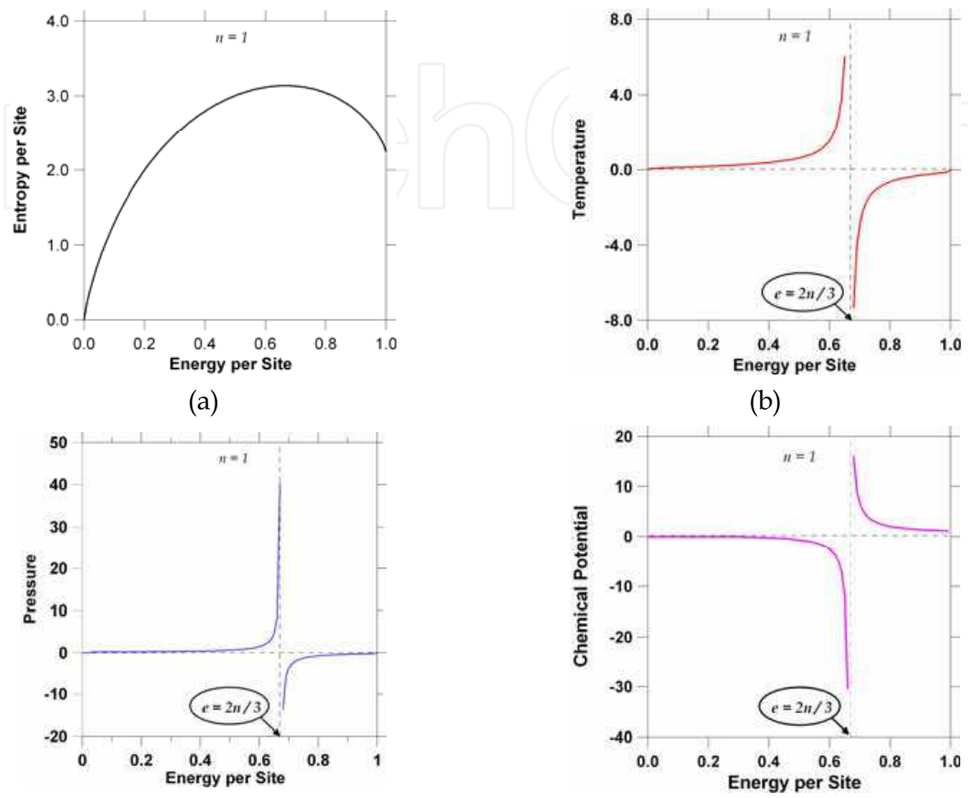

Fig. 6. (a) entropy per site, (b) temperature, (c) pressure, and (d) chemical potential, them all plotted as functions of the energy per site, for $n = 1$.

This figures show that the thermodynamic properties of the lattice gas models have non-classical behaviors. Temperature and pressure, in particular, can assume positive and negative values with an infinite discontinuity at the energy $e = (2/3)n$. This is a consequence of the exclusion principle and of the finite nature of the energy spectrum in these systems. However, it is worth to mention that, in spite of this non classical behavior, for small values of n (that is, in the low density limit) the relation between pressure and temperature can be written as the state equation of an ideal gas:

$$P = -T\sum_{\alpha}\ln(1-n_{\alpha}) \quad \xrightarrow[n\to 0]{} \quad P = nT \tag{16}$$

This result is an indication that, under restricted conditions, the lattice gas may be useful as a model of a classical gas. Other equilibrium thermodynamic properties, such as the specific heat and compressibility, can also be computed from the equilibrium distribution densities.

2.2 Qualitative Hydrodynamic Behavior of the 9-Velocity Lattice Gas

Here we present the results of three different computer simulations we carried out to test the hydrodynamic behavior of the 9-velocity lattice gas model at a qualitative level. The first two simulations show that the model gas behaves as expected in flows past fixed obstacles, and the last one tests the model ability to simulate wave phenomena.

Simulation of flows past fixed obstacles. Figures 7 show the sequences of velocity field sketches obtained from the simulation of the flow past a solid bar (left) and a wedge (right), respectively. A lattice with 300 x 200 sites was used. No gravity neither heating effects were considered. We imposed a flow by initially putting particles at random in the upwards directions ($\mathbf{e}_0$, $\mathbf{e}_1$, and $\mathbf{e}_2$) with an average number of particles per site $n = 2.7$. Particles leaving the top row were introduced in the bottom row randomly but moving upwards. The obstacle operator was defined in the other vertical sides of the lattice and on the obstacle boundary in order to simulate a no-slip condition at the collective level. Both sequences correspond to 2000 time steps of the automaton evolution. Each velocity field was constructed from the experimental distribution functions defined as averages over cells containing 7x7 lattice sites. The left hand sequence shows two vortexes opposite to each other growing past a horizontal bar as time proceeds, such as it is expected for this flow for Reynolds numbers within a certain range. Note also the fluid velocity goes to zero on solid boundaries. In the sequence of the flow past the wedge, it is interesting to observe how the presence of solid wall at right side of the channel forces the development of an adjacent vortex although no obstacle is located there. It would not occur if the system could extend infinitely in the horizontal direction.

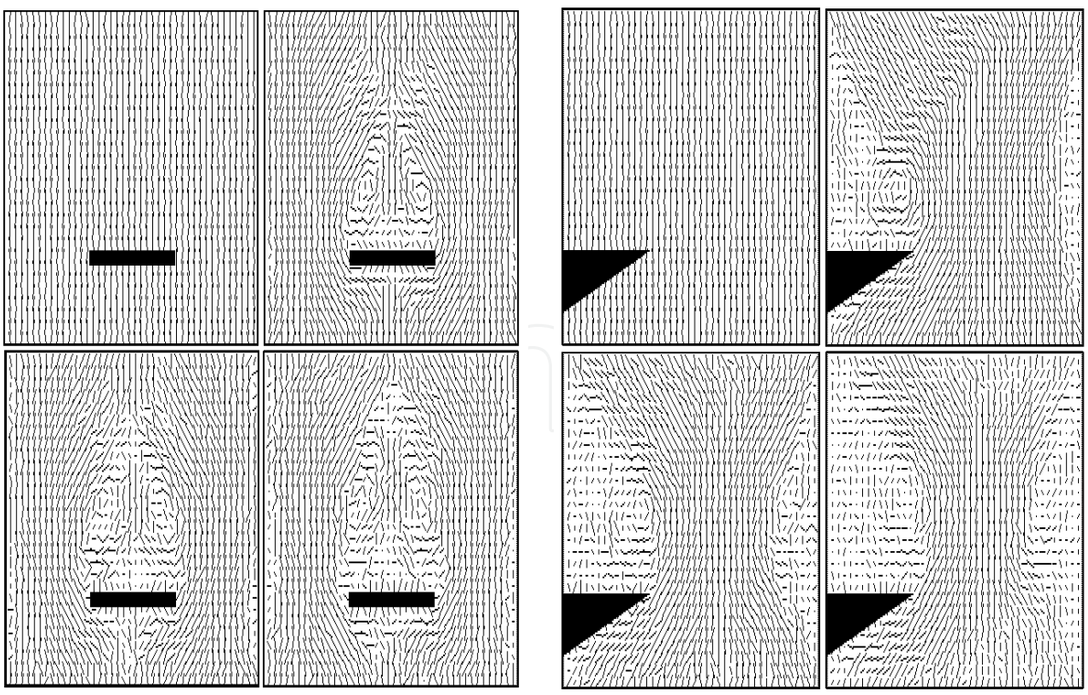

Fig. 7. Lattice gas simulation of the flow past a horizontal bar (left) and a wedge (right), along a vertical channel. No gravity neither heating effects were included.

Simulation of wave phenomena. Figure 8 shows a sequence of the development of a density wave in a closed square box starting from an initial condition where the gas density is uniform everywhere with exception of a centred empty circular hole. A 200 x 200 sites lattice with periodic boundary conditions was used for the computer simulations and no gravity neither heating effects were considered. The gas particles were tossed at random in position and direction of motion keeping an average number of particles per site $n = 2$. Then all the particles located inside a centered circle of given radius were deleted to simulate an empty hole (that is, an initial density perturbation), and the system was allowed to evolve during a number of time steps that was large enough to record the density wave patterns of a full period, at least. As it can be observed, the sequence of density patterns resembles very strongly the wave phenomena which take place in a real gas system.

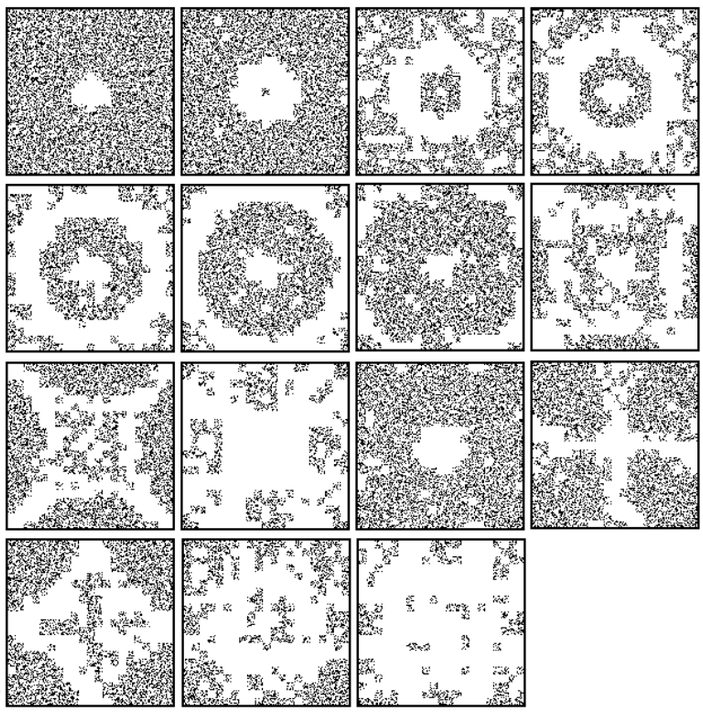

Fig. 8. Lattice gas simulation of a density wave. Initial state: uniform gas with a centred hole (empty) contained in a square box.

2.3 Simulation of Viscous Flows

We have performed two different computer simulations to carry out a simple comparison the 9-velocity lattice gas behaviour against the solutions of the Navier-Stokes equations for the well known Poiseuille and Couette plane flows.

Poiseuille Flow. The steady state flow between two stationary parallel plates driven by an imposed pressure gradient is known as the plane Poiseuille flow. The first simulation we have performed deals with a flow situation more complex than the Poiseuille flow: the relaxation from uniform to equilibrium of the flow between two stationary parallel plates. We used a square lattice with side length $L = 207$ lattice sites. The model gas was contained

between two straight line boundaries at $Y = 0$ (bottom lattice side) and $Y = 207$ (top lattice side). The initial distribution densities were calculated assuming a horizontal flow with uniform velocity $U = 0.15$, an average number of particles per site $n = 2.5$, and an average temperature $T = 10$ (all the magnitudes expressed in the lattice gas units). The obstacle operator **B** was implemented for the top and bottom sides of the lattice in order to simulate a flow along a 2D channel with stationary rigid walls. Periodic boundary conditions were imposed on the other two lattice sides, such that no pressure gradient was present along the channel and the evolution of the system was influenced only by the rigid boundaries. The transversal average velocity profiles are shown in Figure 9. Here we can observe, in agreement with the solution of the Navier-Stokes equations for the plane Poiseuille flow, how a parabolic velocity profile decreases with time, indicating dissipation of momentum and energy due to the collisions of the particles each other and with the solid boundaries.

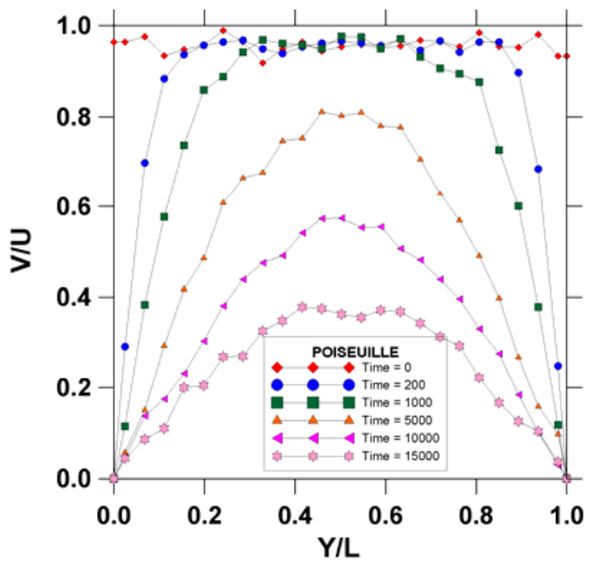

Fig. 9. A non-steady Poiseuille flow. Relaxation from uniform to rest of a 2D flow between two stationary parallel plates.

Couette Flow. The steady state flow between two parallel plates in relative motion is known as the plane Couette flow (see Figure 10 (left)). We performed a lattice gas simulation of the development of a plane Couette flow in two dimensions. A square lattice with side length $L = 207$ lattice sites was considered. The initial distribution densities were calculated by assuming that the gas is initially at rest with an average number of particles per site $n = 2.5$ and an average temperature $T = 10$ (in the lattice gas units). The model gas was contained between two straight line boundaries at $Y = 0$ (top lattice side) and $Y = 207$ (bottom lattice side). The obstacle operator **B** was implemented for the bottom side of the lattice in order to simulate a stationary rigid wall. A uniform in average horizontal velocity, $U = 0.15$ (in the lattice gas units), was imposed at the first five top rows of lattice sites to simulate a moving plate. Periodic boundary conditions were imposed on the left and right sides of the lattice (this way, the pressure gradient is zero and that the only forcing on the fluid is forcing due to the moving plate). Ten computer simulations, 15,000 time-steps each, were done with the same initial and boundary conditions. The vertical profiles of average velocity were

obtained for time-steps *t =0, 200, 1000, 5000* and *15000*. These profiles are shown in Figure 10. It can be observed in this figure how, due to the viscosity of the lattice gas, the relative velocity between the top and bottom boundaries gradually forces the movement of the model gas (initially at rest) with a clear tendency towards a linear profile. The viscosity makes the fluid stick to the boundary which is why a shear develops within the interior of the fluid. The time evolution of the simulated velocity profile and its asymptotical form are in agreement with the solution of the Navier-Stokes equations for the development from rest to the steady state of the laminar viscous flow between two parallel rigid plates in uniform relative motion (Batchelor, 1967).

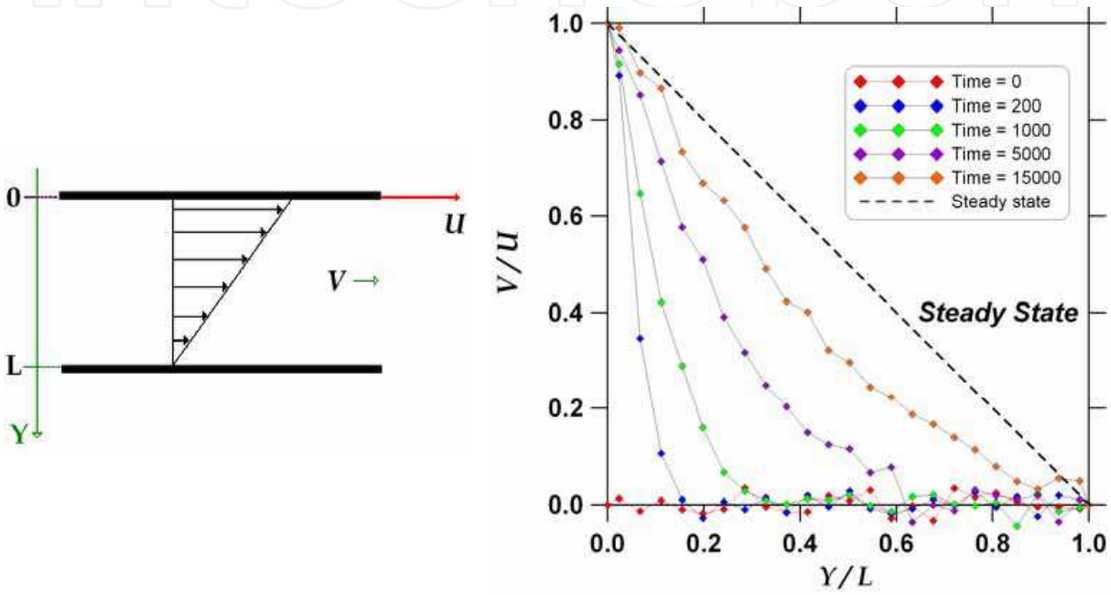

Fig. 10. Simulation of the Couette flow. Development from rest to the steady state.

3. Lattice Gas Simulation of Wind Fields

One of the main attractive features of the fluid flow simulation with lattice gas models is its ability to handle complex initial and boundary conditions. This is one of the reasons why we considered convenient to investigate the lattice gas possibilities as an alternative approach for solving the problems (both diagnosis and prognosis) of the wind fields prevailing in topographically complex terrains.

A simple meteorological outline of the wind field diagnosis problem is as follows: At the stations of an atmospheric monitoring network, the meteorological variables of pressure, temperature, and wind speed and wind direction are measured at a number of sites spatially distributed over a topographically complex and relatively large region. So, for any given time, the meteorological data registered at the network stations are to be used offline to estimate the wind velocity at any given point within the spatial domain of interest.

Within the framework of the computational fluid dynamics, the approach to the problem is focused on solving numerically the set of balance differential equations to find out the steady state of the system that complies the constraints imposed by the boundary (complex topography) and time asymptotic (measured values) conditions. Otherwise, in the lattice gas

approach to the wind field estimation problem, the available data of pressure, temperature and wind velocity are used to compute the steady state distribution functions, $n_\alpha(\mathbf{r}_i)$, for a given number of control lattice sites $\mathbf{r}_i$. The topographic data, on another hand, are used to define some special domains of lattice sites which are to be forbidden to the particles of the model gas; these particular domains are defined in order to represent the fixed obstacles in the computer simulations, and the obstacle operator will affect the particles arriving to their boundaries. Once the system has been prepared, it is allowed to evolve during a given number of time steps. The number of time steps that the system requires to reach a steady state depends on the size of the lattice and on the number of control points it comprises.
Under equilibrium conditions, the values of the distribution functions at the control points can be computed using the equilibrium formalism of the section 2.1 after an appropriate scaling procedure to express the meteorological data in the lattice gas units. Out of equilibrium, the same approach can be used by assuming local equilibrium conditions and using a constrained perturbation technique in order to satisfy the desired local velocity conditions for a given number of particles per site n. So,

$$n_\alpha = \tilde{n}_\alpha + \delta n_\alpha \ , \quad \sum_\alpha \delta n_\alpha = 0 \ , \quad \mathbf{v}(\mathbf{r},t) = \frac{1}{n}\sum_\alpha c_\alpha \mathbf{e}_\alpha \delta n_\alpha \tag{17}$$

The outputs of the computer simulations are average distribution functions computed over cells of 9 x 9 lattice sites. While the simulation goes on, the average distribution densities, denoted as $f_\alpha(\mathbf{x}, t)$, can be computed as frequently as it is desired for each cell position $\mathbf{x}$, and they are used to calculate the wind velocity $\mathbf{v}(\mathbf{x}, t)$ as follows:

$$\mathbf{v}(\mathbf{x},t) = \frac{1}{f}\sum_\alpha c_\alpha \mathbf{e}_\alpha f_\alpha(\mathbf{x},t), \quad f(\mathbf{x},t) = \sum_\alpha f_\alpha(\mathbf{x},t) \tag{18}$$

Before considering a real and practical study case, a few computer simulations were carried out to test the lattice gas capabilities in modelling of situations of turbulent flow similar to those ones which prevail in the atmospheric surface layer. Our main concern was to find out the ability of the model to reproduce the well known quasi-logarithmic wind velocity profile

$$u(y) = \frac{u_*}{\kappa}\left[\ln\left(\frac{y}{y_0}\right) - \Psi_M\left(\frac{y}{L}\right)\right] \tag{19}$$

where u is the mean wind velocity, u^* is the friction velocity, κ is the von Karman constant, y is the height over the earth surface, y_0 is the roughness length, L is the Monin-Obukhov length, and Ψ_M is a universal function which takes into account corrections to the logarithmic profile due to the atmospheric stability conditions (Garrat, 1992).
The computer simulations were performed with a lattice that comprised 207 x 207 sites. Periodic boundary conditions were imposed on the left and right sides of the lattice. The bottom side ($y = 0$) was filled with small obstacle towers whose heights were chosen randomly to simulate a roughness length equal to 5 % of the lattice side length ($y_0 \sim 10.35$).

The lattice gas was assumed initially at rest on the average, with a number of particles per site $n = 2.5$, and a temperature $T = 10$. In the top lattice side ($y = 207$) it was imposed a fixed horizontal velocity U using the first five lattice rows as control points. Ten computer simulations, *35000* time steps each one, were made for $U = 0.1, 0.3, 0.5, 0.7$ and 0.9 with the same initial and boundary conditions. In Figure 11 there are shown the mean wind velocity profiles obtained for $U = 0.3$ and times $t = 0, 1000, 5000, 10000, 20000, 25000, 30000$ and 35000. In this figure we note that the system reached the steady state flow conditions (continuous straight line), that the steady state velocity profile is linear such as it is predicted by the Navier-Stokes equations in the laminar case (Batchelor, 1967), and that, because the roughness of the bottom lattice side, the wind velocity became zero near (but not at) the surface ($V/U \sim 0$ at $Y/L \sim 0.058$).

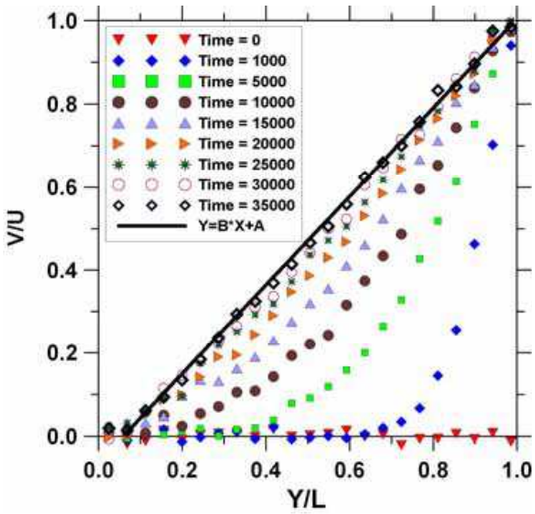

Fig. 11. Lattice gas simulation of the Couette flow development from rest to the steady state, when a no null roughness length is associated to the bottom stationary plate.

In figure 12 there are shown the wind velocity profiles for $t = 35000$ and $U = 0.1, 0.3, 0.5, 0.7$ and 0.9, and it can be observed that the velocity profile deviates from the linear case as U increases. This is what really happens on the transition of the flow from a laminar state to a turbulent one. For $U = 0.9$ the velocity profile is, in fact, quasi-logarithmic. In this figure, the solid curve corresponds to the equation (19) with $u^*/k = 0.3$ and Ψ_M given by

$$\Psi_M = a(y - y_0)\ln\left(\frac{y+1}{b(y-1)}\right) \tag{20}$$

where $y_0 = 10.5$, $a = 0.2$ and $b = 1.016$. Although the 9-velocity lattice gas model may have a clearly non-classical behaviour at energies higher than $2n/3$, the results of the various simulations that we have performed show that it can be useful for some meteorological applications, such as the wind field estimation problem, if it is handled carefully. The ranges of values of the density and the energy which are safe for a particular practical application might be identified previously.

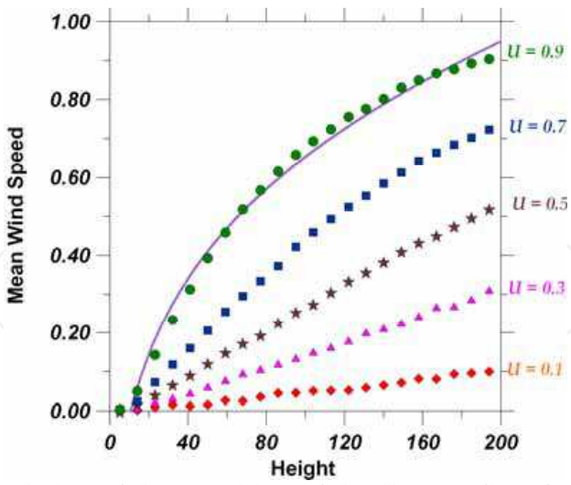

Fig. 12. Lattice gas simulation of the transition of the Couette flow from a laminar state to a turbulent one.

4. The Main Wind Circulation Events at Mexico City in 1994

In this section, the wind circulation events which occurred in the Mexico City Metropolitan Area throughout the year 1994 are identified, described, and organized. For the purposes of the present work, the main goal of this task is to have good enough criteria to identify and select, among the 8760 wind circulation possibilities (in an hourly base), the most important scenarios for the computer simulations. A very recent description of the methodology we have applied to select our simulation scenarios was reported briefly by M. S. Jimenez, A. T. Celada and A. Salcido in 2008 (Jimenez et al, 2008), and more precisely by A. T. Celada and A. Salcido in 2009 (Celada & Salcido, 2009).

4.1 Meteorology Databases

In 1994, with the economical support of the Mexico City government, under the initiative COPERA, personnel of the Instituto de Investigaciones Eléctricas (IIE) carried out, from June to September, the first experimental campaign of micrometeorological measurements in surface, simultaneously in 4 sites of the Mexico City Metropolitan Area (Salcido et al, 1994). For this purpose, the MCMA was geographically divided in the quadrants North-East (NE), North-West (NW), South-East (SE), and South-West (SW), taking the Zócalo of Mexico City as origin. One micrometeorological station was installed at each quadrant. In Figure 13, there are shown the relative positions of the micrometeorological stations installed by the IIE in the MCMA. Each station was equipped with an ultrasonic 3D anemometer-thermometer, and conventional sensors for temperature, pressure, relative humidity, and solar radiation. The 3D wind velocity components were measured with a 10 Hz sampling rate by the ultrasonic anemometer, and the other variables were measured at 1Hz. Averages over 10 minute periods were computed for all variables.

On another hand, since 1984, it is operating an automatic atmospheric monitoring network (RAMA, for its name in Spanish) in Mexico City and its surroundings, financed by the local governments. In 1994, the RAMA comprised 32 stations, 10 of which with the ability to measure meteorology (wind speed, wind direction, temperature, and relative humidity),

providing public reports of the hourly average values. In the RAMA database, the 1-hour averages are identified by the number of the hour of the day. The RAMA historical database is now available on the internet site http://www.sma.df.gob.mx/simat/home_base.php. In Figure 14, the seven meteorological stations of the RAMA with the best performance in 1994 are shown. In Table 1, we reported the numbers of hours, month by month, for which the seven selected RAMA stations were operating simultaneously with a 100% performance.

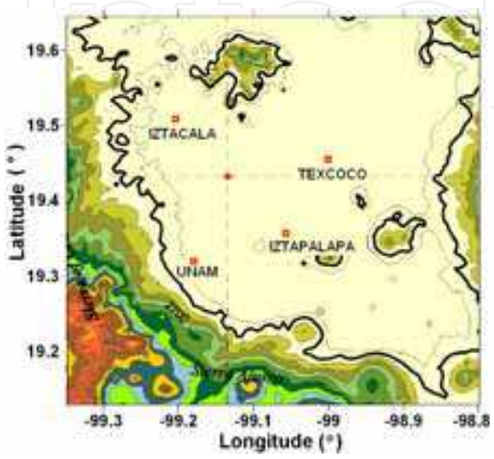

Station Name	MCMA Quadrant	UTM (Zone 14)	
		Easting	Northing
Texcoco	NE	499.562	2151.650
Iztacala	NW	480.094	2158.647
UNAM	SW	481.587	2136.731
Iztapalapa	SE	492.298	2140.504
Zócalo	Origin	486.011	2148.699

Fig. 13. Relative positions of the four stations that the IIE installed in the MCMA to perform a micrometeorological campaign from June to September in 1994. In the table, the positions are expressed in UTM coordinates (in Km).

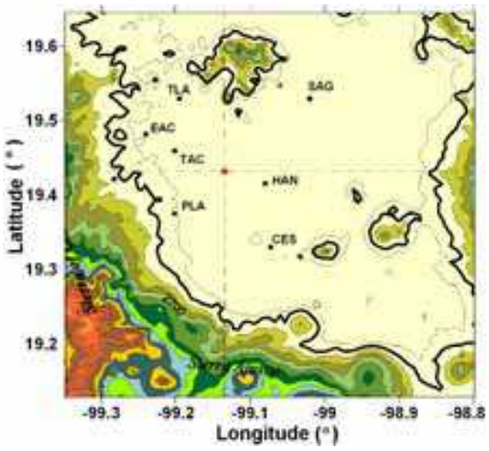

ID	Station Name	MCMA Quadrant	UTM (Zone 14)	
			Easting	Northing
SAG	San Agustin	NE	496.794	2159.651
TLA	Tlanepantla	NW	478.521	2159.233
EAC	ENEPAcatlan	NW	474.580	2154.443
TAC	Tacuba	NW	478.774	2151.088
PLA	Plateros	SW	480.249	2139.878
HAN	Hangares	SE	491.251	2147.420
CES	Cerro de la Estrella	SE	492.909	2137.308

Fig. 14. Relative positions of the seven meteorological stations of the RAMA with the best performance in 1994. In the table, the positions are expressed in UTM coordinates (in Km). The official IDs and the quadrants to which they belong are also reported.

Month	JAN	FEB	MAR	APR	MAY	JUN	JUL	AUG	SEP	OCT	NOV	DEC
Hours	411	125	357	402	316	292	377	304	492	306	383	249

Table 1. Monthly distribution of the hours for which the selected RAMA stations were operating simultaneously with a 100% performance.

Although the field campaign carried out by the IIE took place within the period of the summer rainy season of 1994, the existence of two independent sources of meteorology data (IIE and RAMA) for the same period did open, for the first time, an opportunity particularly interesting for the purposes of the characterization and modelling of the Mexico City winds. One of the databases can be used as input for the models, and the other one may be useful for the comparison purposes.

4.2 The Wind Direction States Representation Model

By considering the MCMA divided in quadrants, such as it was done in the previous subsection, a very simple description of its wind circulation events can be carried out. At a given time, we define the *wind direction state* of the MCMA as the set of the four wind direction sectors (N≡0, NE≡1, E≡2, SE≡3, S≡4, SW≡5, W≡6 or NW≡7) that correspond to the wind direction average values at the MCMA quadrants, which are computed from the wind speed and wind direction values registered by the RAMA stations located inside each quadrant. So, at any given time, the wind direction state at the MCMA may be expressed as a 4-digits octal number ranging from 0000 to 7777 (from 0 to 4095, in base 10). It is a mapping of the infinite possibilities of the wind circulation events at the MCMA (each expressed by an spatial distribution of the wind velocity) into the 4096 possible wind direction states. The highest order digit represents the sector of the mean wind direction at the quadrant NE, and the next digits represent, in decreasing order, the sectors of the mean wind directions at the quadrants NW, SW, and SE, respectively. So, the octal number 1070 (decimal 568) represents the wind direction state with North-easterly wind at the NE quadrant, Northerly wind at the NW quadrant, North-westerly wind at the SW quadrant, and Northerly wind at the SE quadrant, as it is shown in Figure 15.

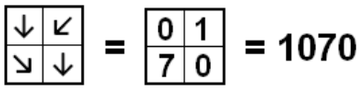

Fig. 15. Octal representation of a MCMA wind direction state. It has winds from NE, N, NW and N, at the NE, NW, SW and SE quadrants, respectively.

The frequency distribution of the wind direction states (normalized to 1 or, equivalently, to 100) constitutes a convenient way to distinguish which of them can be observed at the study area under different conditions, and also for conveying their probabilities of occurrence. It will be referred as the *density of states of wind direction*. On another hand, the 4096 wind direction states can be organized in groups by taking into account the following three characteristics of any wind direction state:

- θ: the wind direction sector of the average value of the four mean wind directions of the quadrants (it has 9 possible values: Ø, N, NE, E, SE, S, SW, W, NW)‡;
- ω: the sign of the vorticity of the state (3 possibilities: anticyclonic = -1, null vorticity = 0, and cyclonic = 1); and
- γ: the sign of the divergence of the state (3 possibilities: convergent winds = -1, null divergence = 0, and divergent winds = 1).

‡ The symbol Ø is used to indicate that the wind directions at the quadrants are opposite in pairs, and their average is not defined. The state 1054 (octal) is an example.

The concept of wind direction state, with its three associated attributes, (θ, ω, γ), may be understood as a meso-β scale representation model of the wind circulation events. Refined versions of this simple representation model may be implemented. Within the framework of this representation, the state illustrated in the Figure 15 belongs to the group of the North-Cyclonic-Convergent states, denoted by the triad (θ,ω,γ) = (N, 1, -1). There are 81 (θ,ω,γ)–groups in which the 4096 wind direction states can be organized in response to the particular wind driving forces (such as, the topography and the meteorological conditions) which prevail at the MCMA. So, the mechanisms which drive the winds at the MCMA constitute the main influence factors to the population of its (θ, ω, γ)–groups.

4.3 The 1994 Mexico City Wind Direction States

From the RAMA 1994 database, we found that the seven stations selected for our study were operating simultaneously with 100% performance only during 4014 of the 8760 possible hours, which were distributed throughout the year as described in Table 1. Among these events, only 985 wind direction states were different each other. In Figure 16, the distribution of frequencies of the wind direction states normalized to 100 (i.e. the density of states of wind direction) is shown for the 4014 hours.

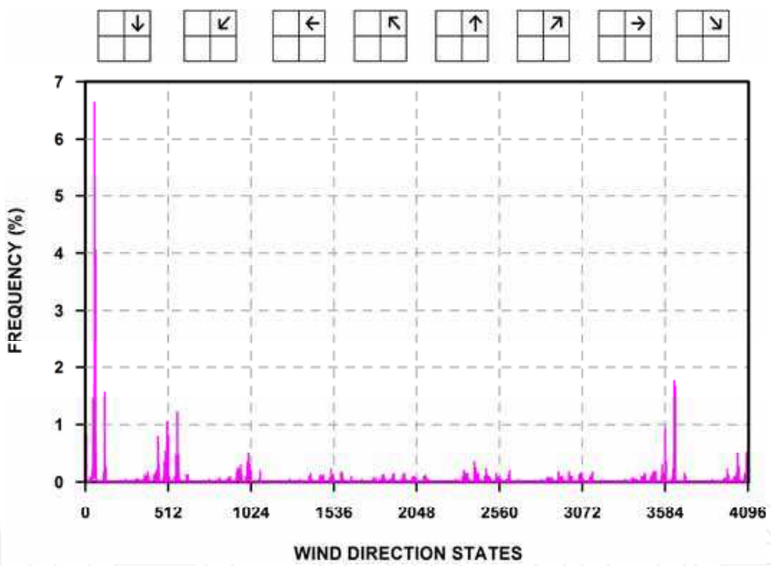

Fig. 16. The density of states of wind direction of the MCMA for the 1994 year. Here, the states are expressed in the decimal base (0 … 4095). The plot contains information of 4014 hours of the total 8760 possible hours.

The plot in this figure shows eight packets of 512 states each, ordered according to the wind direction sector at the quadrant NE. This quadrant is particularly important because its North side is the main opening of the MCMA to the wind flows, as it was shown in Figure 1. The states from 0 to 1023 and from 3584 to 4095 represent wind events with a Northerly, North-easterly or North-westerly flow component at the NE quadrant, while the states from 1536 to 3071 represent wind events with a Southerly, South-westerly or South-easterly flow component at the same quadrant. The wind direction states with the

highest frequencies did belong, in order of population, to the packets 0-511, 3584-4095, and 512-1023, whose states showed, respectively, a Northerly, North-westerly or North-easterly flow component at the NE quadrant. The individual states with the highest frequencies, in decreasing order, were 56, 63, 0, 57, 3640, 55, 3647, 120, 48, 568, 1 and 504 (see Figure 16). These observations are in agreement with the information reported by Secretaria del Medio Ambiente of Mexico City about the predominant Northerly/North-easterly winds at MCMA (SMA-GDF, 2006). Moreover, wind flows from these directions were also described by Doran and collaborators in 1998 (Doran et al., 1998) and by Doran and Zhong in 2000 (Doran & Zhong, 2000) as Northerly and/or North-easterly winds from the Mexican Plateau. Table 2 contains a representation of the wind direction states with the highest frequencies and the respective (θ,ω,γ)–group each belongs to.

STATE (Decimal)	FREQ (%)	GROUP (θ, ω, γ)	STATE (Decimal)	FREQ (%)	GROUP (θ, ω, γ)	STATE (Decimal)	FREQ (%)	GROUP (θ, ω, γ)
56	6.65	(N, 1, -1)	3640	1.77	(NW, 0, 0)	48	1.44	(N, 0, -1)
63	4.06	(NW, 1, -1)	55	1.72	(NW, 1, -1)	568	1.22	(N, 1, -1)
0	3.71	(N, 0, 0)	3647	1.67	(NW, 1, 1)	1	1.15	(N, -1, -1)
57	1.77	(N, 0, -1)	120	1.57	(N, 1, 0)	504	1.05	(NW, -1, -1)

Table 2. The wind direction states of the MCMA which had the highest frequencies in 1994.

Because of the obvious differences between the wind driving forces which prevail during diurnal and nocturnal conditions, the daytime occurrence frequencies of the wind direction states differ from those of nighttime situations. To study these differences, we organized the 1994 wind direction states in 6-hour packets: Night (hours 1-6), Morning (hours 7-12), Afternoon (hours 13-18), and Evening (hours 19-24). In Figure 17, the occurrences of the states with the highest frequencies at the density of states are presented for the annual case, and also for the night, morning, afternoon, and evening 6-hour packets. In this figure we observed that, in 1994, the behaviour of the state 56, the state with the highest annual frequency, shows an occurrence frequency that grows as one moves from night hours (1-6 packet) to the evening hours (19-24 packet). Otherwise, for the state 63, that one with the second highest annual frequency, its occurrence frequency decreases as one moves from the night to the afternoon 6-hour packets, and then it grows, recovering at the evening packet the value it had at the night packet. Finally, the behaviour of the state 0, which got the third highest annual frequency, is opposite to that of the state 63: it occurrence grows from the night to the afternoon packets, and then it decreases at the evening hours. The behaviour of these particular MCMA wind direction states seems to follow the 24 hours periodicity of the sunlight. Other states, like the state 120, seem to be insensible to this periodicity. It is worth of mention that our previous observations show that, in spite of its simplicity, our meso-β scale representation model is able to reflect the main features of the wind circulation events that prevail in the MCMA, or at least some of them. It must be underlined, however, that the

results of this state model will be sensible to the number and the spatial distribution of the stations at the quadrants, particularly for small or poor distributed meteorological networks.

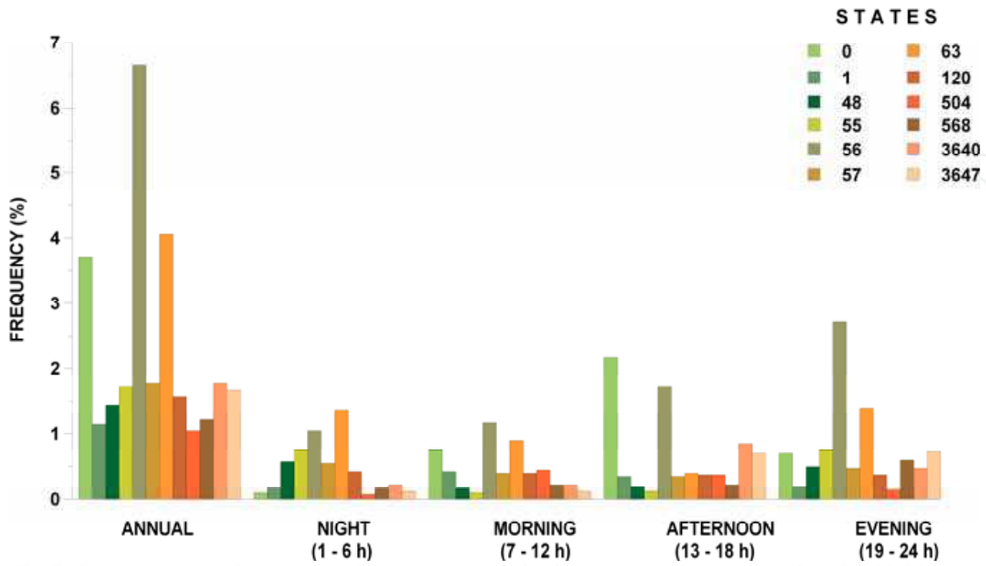

Fig. 17. Behaviour of the most frequent wind direction states of the MCMA in 1994. Comparison of the annual frequency distribution with the corresponding to the night, morning, afternoon, and evening 6-hour packets.

In addition, we organized the 1994 MCMA wind direction states in (θ, ω, γ)–groups; their population percentages are shown in Figure 18. In this figure, it can be observed that the most populated groups in 1994 were the North-Cyclonic-Convergent (N, 1, -1) with the highest population, the Northwest-Cyclonic-Convergent (NW, 1, -1) with the second highest population, and the Northwest-Anticyclonic-Convergent (NW, -1, -1) in third place. The (θ, ω, γ)–groups with the smaller populations were those with θ = E, Ø and SE, almost independently of the other attributes (ω and γ).

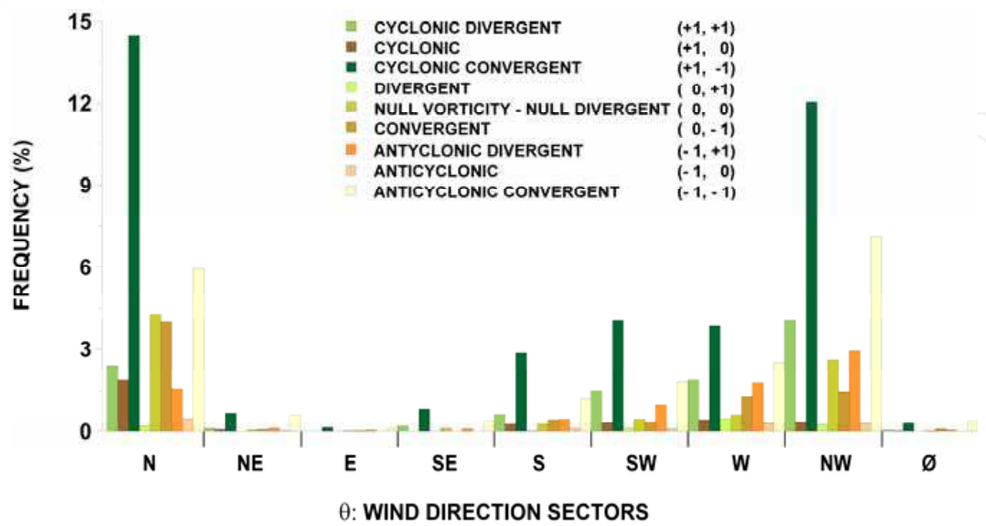

Fig. 18. Frequency distribution (or population) of the (θ, ω, γ)–groups for the year 1994.

5. Lattice Gas Simulation of Mexico City Wind Fields

In this section, it is described and discussed the application of the 9-velocity lattice gas model in estimating the MCMA wind field for some particular wind circulation events which occurred at both daytime and nighttime hours of the 1994 summertime. The comparison of the simulation results against wind velocity data registered at the stations of the official atmospheric network (RAMA) of Mexico City, are also presented.

5.1 Selection of the Mexico City Wind Scenarios

In Section 4, we have seen that from the wind circulation events which occurred in the Mexico City Metropolitan throughout the year 1994, those ones with a Northerly, Northeasterly or Northwesterly wind at the NE quadrant were found with the highest frequencies. Following this observation, for the purpose of applying the 9-velocity lattice gas model to simulate the Mexico City Metropolitan Area wind field, we chose as simulation scenarios the wind events which prevailed at the 9:00 (morning), 15:00 (afternoon) and 21:00 (evening) hours (LST) of the days July 31 and August 26, 1994. The wind direction states of the chosen wind scenarios were computed, separately, with the data of the RAMA stations and the data of the IIE campaign; both results are reported in Table 3. Here we can observe that the wind direction states of the six chose scenarios belong to the first two packets of the density of states (Figure 16). It is interesting to observe in Table 3 that, although very similar (particularly for the morning and afternoon wind scenarios), the wind directions states obtained with the IIE database differ from those found with the RAMA data. The main reason for these differences is that, whilst the RAMA database was prepared with data of a total of seven stations, the IIE database was obtained with data of only one station at each quadrant of the MCMA. Moreover, at the quadrants, the station positions of the IIE network did not coincide with positions of RAMA stations.

For each one of the wind scenarios chosen for computer simulation, the input database for the wind field lattice gas model was prepared (such as it was outlined in Section 3) from the data of pressure, temperature and wind velocity taken from the four meteorological stations of the IIE network. The data of the RAMA network were kept as information of reference for the comparison purposes of the study. Once scaled to fix the lattice gas units, the meteorological data of the IIE stations were used to find the perturbations of the local equilibrium distribution densities congruent with the velocity control values at the lattice sites that represent the positions of the stations.

5.2 Simulations and Results

The simulation spatial domain, a rectangular region of the MCMA with side length of 70 Km in the west-east direction and 60 Km in the north-south direction, was represented by a lattice containing 396 x 324 sites. The boundary conditions at the free lattice sides were imposed by assuming that the values of pressure, temperature and wind velocity were there equal to the corresponding average values over the four control sites. In all the other lattice sites, the lattice gas was assumed, on the average, as initially at rest and under conditions of thermodynamic equilibrium. For each wind scenario, the lattice gas model was run five times, 5000 time steps each. The simulated wind velocity distribution for each scenario was computed from the distribution densities obtained as a direct output of the computer simulation.

Date: 1994/07/31				
	RAMA STATIONS		IIE STATIONS	
LOCAL TIME	STATE (Decimal)	GROUP (θ, ω, γ)	STATE (Decimal)	GROUP (θ, ω, γ)
09:00	448 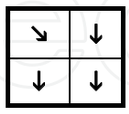	(N, -1, -1)	0 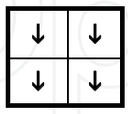	(N, 0, 0)
15:00	64 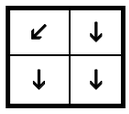	(N, 1, 1)	1 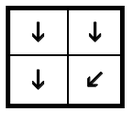	(N, -1, -1)
21:00	318 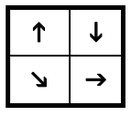	(W, 1, 1)	10 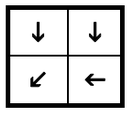	(NE, -1, -1)

Date: 1994/08/26				
	RAMA STATIONS		IIE STATIONS	
LOCAL TIME	STATE (Decimal)	GROUP (θ, ω, γ)	STATE (Decimal)	GROUP (θ, ω, γ)
09:00	57 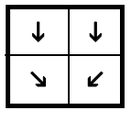	(N, 0, -1)	1 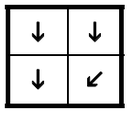	(N, -1, -1)
15:00	64 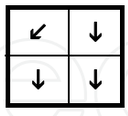	(N, 1, 1)	0 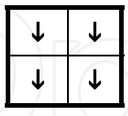	(N, 0, 0)
21:00	553 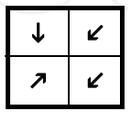	(N, -1, - 1)	556 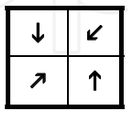	(Ø, +1, -1)

Table 3. The MCMA wind direction states which prevailed the days (July 31 and August 26, 1994) selected for the lattice gas simulation of the Mexico City wind field.

A comparison between the wind direction states produced by the lattice gas simulations of the chosen wind scenarios, and the wind direction states obtained from the data of the RAMA stations, are shown in Table 4. In this table, in general, it is observed a quite good

qualitative agreement between both sets of wind direction states, excepting those for the 21:00 h scenario of the first day. However, as we will see later, the stations Tlanepantla and Tacuba of the RAMA network did not report the wind data that day.

Date: 1994/07/31				
	RAMA STATIONS		**LATTICE GAS SIMULATION**	
LOCAL TIME	STATE (Decimal)	GROUP (θ, ω, γ)	STATE (Decimal)	GROUP (θ, ω, γ)
09:00	**448** 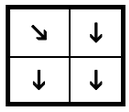	**(N, -1, -1)**	**904** 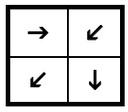	**(N, -1, 0)**
15:00	**64** 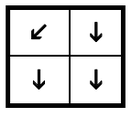	**(N, 1, 1)**	**960** 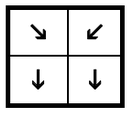	**(N, 0, -1)**
21:00	**318** 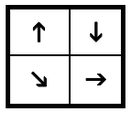	**(W, 1, 1)**	**721** 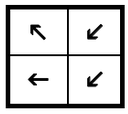	**(E, -1, 1)**

Date: 1994/08/26				
	RAMA STATIONS		**LATTICE GAS SIMULATION**	
LOCAL TIME	STATE (Decimal)	GROUP (θ, ω, γ)	STATE (Decimal)	GROUP (θ, ω, γ)
09:00	**57** 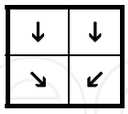	**(N, 0, -1)**	**448** 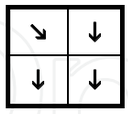	**(N, -1, -1)**
15:00	**64** 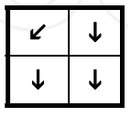	**(N, 1, 1)**	**960** 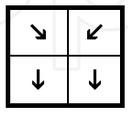	**(N, 0, -1)**
21:00	**553** 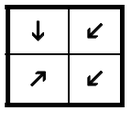	**(N, -1, - 1)**	**960** 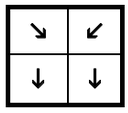	**(N, 0, -1)**

Table 4. Comparison of the MCMA wind direction states obtained from data of the RAMA stations (left) and from the lattice gas simulations (right) for the chosen wind scenarios.

In Figures 19 and 20, sketches of the wind fields estimated for the MCMA are shown. Quantitative results of the wind velocities estimated with the lattice gas model at the sites of the stations of the RAMA network are reported in Table 5. These tables include also the wind velocity data registered at the RAMA stations for the chosen wind scenarios. Of course, it is not surprising that for the four control stations it was found a fair agreement between the measured wind velocity values and those estimated with the lattice gas model. In fact, the lattice sites which were representing these stations in the computer simulations were updated with the velocity control values each time step.

Date: 1994/07/31	09:00				15:00				21:00			
	Measured		Estimated		Measured		Estimated		Measured		Estimated	
Station	WSP (m/s)	WDR (°N)	WSP (m/s)	WDR (°N)	WSP (m/s)	WDR (°N)	WSP (m/s)	WDR (°N)	WSP (m/s)	WDR (°N)	WSP (m/s)	WDR (°N)
IZTACALA	1.00	353	0.95	355	2.50	354	2. 53	354	1.24	356	1.30	356
TEXCOCO	1.92	351	1.97	350	2.51	339	2.55	340	1.35	355	1.36	355
UNAM	0.97	5	1.00	3	1.33	8	1.34	8	0.45	25	0.49	24
IZTAPALAPA	0.71	4	0.78	0	2.23	47	2.30	47	1.79	71	1.83	70
TLANEPANTLA	----	----	1.55	313	----	----	4.13	318	----	----	4.13	318
SN. AGUSTIN	1.70	339	2.88	30	2.59	347	4.40	25	2.55	6	2.34	33
ACATLAN	1.21	300	0.88	305	3.53	32	2.19	334	3.40	200	1.52	170
TACUBA	----	----	0.38	297	----	----	2.16	326	----	----	1.23	153
HANGARES	1.70	324	2.53	24	4.10	15	3.30	14	2.41	216	2.00	40
C. ESTRELLA	1.21	2	1.08	338	2.28	26	1.79	348	1.88	341	0.43	9
PLATEROS	1.16	352	0.97	21	2.37	352	1.24	31	2.41	311	1.00	45

Date: 1994/08/26	09:00				15:00				21:00			
	Measured		Estimated		Measured		Estimated		Measured		Estimated	
Station	WSP (m/s)	WDR (°N)	WSP (m/s)	WDR (°N)	WSP (m/s)	WDR (°N)	WSP (m/s)	WDR (°N)	WSP (m/s)	WDR (°N)	WSP (m/s)	WDR (°N)
IZTACALA	2.11	2	2.13	1	3.92	0	3.85	0	1.92	9	1.97	7
TEXCOCO	2.73	14	2.79	13	5.12	351	5.19	351	3.83	54	3.92	53
UNAM	1.64	1	1.75	2	2.03	351	2.01	353	1.19	208	1.23	207
IZTAPALAPA	1.63	53	1.68	52	4.29	6	4.41	6	1.89	193	1.95	193
TLANEPANTLA	2.59	17	2.96	323	4.87	30	5.11	324	2.91	20	2.02	320
SN. AGUSTIN	2.50	16	2.67	18	4.91	343	6.14	24	3.17	25	2.50	12
ACATLAN	2.19	41	2.03	334	3.84	72	2.67	340	2.95	49	1.27	324
TACUBA	2.41	359	1.70	308	3.62	343	2.69	311	2.91	321	1.07	315
HANGARES	2.82	46	1.82	21	6.69	9	4.68	22	3.13	44	1.36	35
C. ESTRELLA	----	----	1.81	345	----	----	3.18	347	----	----	0.89	314
PLATEROS	1.56	329	1.35	351	2.37	353	2.20	12	1.52	243	0.46	25

Table 5. Comparison of the values of wind speed and wind direction measured at the RAMA stations and estimated with the lattice gas model.

Although the comparison with the velocity values measured at the RAMA stations is not direct neither trivial because many of them were strongly influenced by the big obstacles in the surroundings, the velocity values estimated with the lattice gas model at the sites of the RAMA stations show a reasonable agreement with the available experimental data. In fact, on the average, the wind velocity values estimated with the model differ from the experimental ones in a 30 per cent, very roughly. However, a more carefully inspection evidences situations where the agreement is quite good, as it is the case for the ACATLAN station at 9:00 h of the first day, or the SAN AGUSTIN station also at 9:00 h of the second day, or at the PLATEROS station at 15:00 h also the second day. In general, the worst estimations occurred near to the solid boundaries, and we think this is due to the strong boundary conditions we have imposed there (particles arriving to solid boundaries are

strictly constrained to invert its direction of motion). Of course, it is necessary to explore the effects of some other possibilities of boundary conditions at the solid obstacles at large spatial scales.

On another hand, it must be underlined that the simulations we carried out were two dimensional; this means, in particular, that the presence of the urban buildings has be neglected completely, and that the conservation of the number of particles in the microdynamics of the model may lead to lateral flows under wind forcing conditions that, in reality, could be driving vertical flows. It may be the case when the wind direction states belong to highly convergent or divergent winds, such as those thermally produced by the heat island effect, or in combination with the particular topographic features of the MCMA that define a closed region.

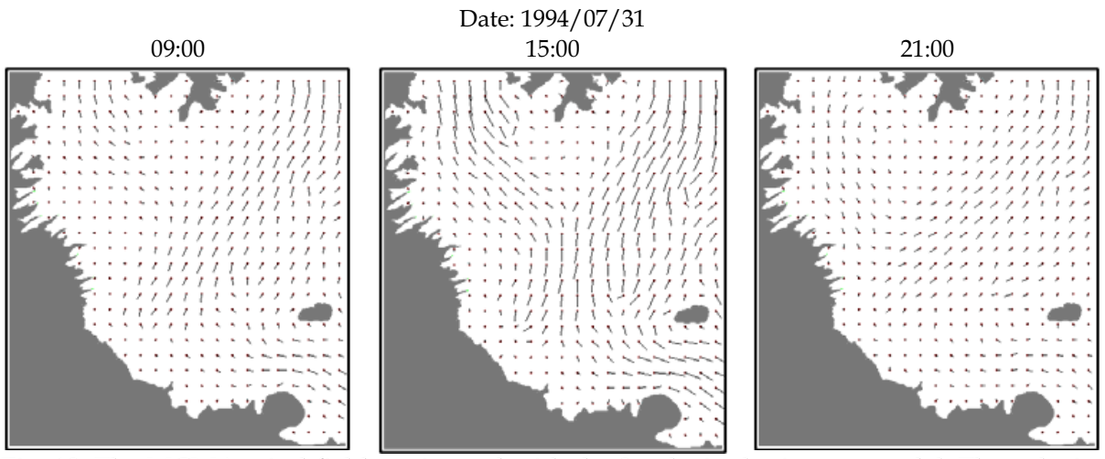

Fig. 19. The MCMA wind fields estimated with the 9-velocity lattice gas model. The velocity vectors are represented by needles, each extending from the centre (dot) of a cell that comprises 9x9 lattice sites. Date: July 31, 1994.

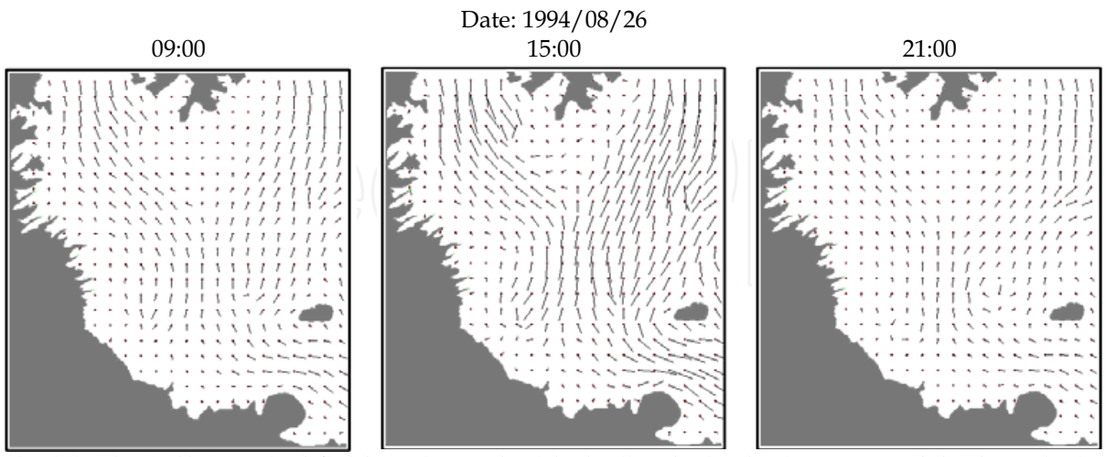

Fig. 20. The MCMA wind fields estimated with the 9-velocity lattice gas model. The velocity vectors are represented by needles, each extending from the centre (dot) of a cell that comprises 9x9 lattice sites. Date: August 26, 1994.

6. Conclusion

In this chapter we have presented an application of the 9-velocity lattice gas model as an alternative and innovative approach to the wind field estimation problem in two dimensions. The computer simulations performed to test the model showed off that it is capable to reproduce steady and non steady laminar and turbulent well known flow situations. In particular, it was able to reproduce the typical surface layer quasi-logarithmic wind profile. This wind field model, however, is still in an experimental phase, but, as an important part of its validation and calibration, we have applied it to estimate the wind field of the Mexico City Metropolitan Area for daytime and nighttime conditions of the 1994 summertime, specifically for the hours 9:00, 15:00 and 21:00 (LST) of the days July 31 and August 26. The results we have obtained through the computer simulations for this study case, as well as for the preliminary test simulations, have shown a reasonable agreement (both qualitative and quantitative) between the measured and estimated velocity values, and it suggests strongly that the model could be, in fact, a very useful tool for a wide variety of practical fluid flow applications.

There exist, however, some important features of the 9-velocity lattice gas model that one must keep in mind in developing practical applications with it. The equilibrium behaviour of the model is not the classical one that an ordinary fluid presents. The entropy as function of energy has a maximum value for any given number of particles per site, and this behaviour is reflected in the dependence on energy of the temperature and pressure, which may assume not only positive values, but also negative ones. However, as the number of particles per site goes to zero (i.e. in the limit of low densities), the behaviour of the model seems to be closer to the classical one. On other hand, it is very important to extend the model to three dimensions in order to consider some of the important and frequent wind scenarios that prevail at Mexico City and its surroundings (for example, the thermally driven and upslope and downslope winds). From the technical point of view, it is not a difficult task, but the development of very fast codes will be important to keep reasonable the duration of the model runs.

7. References

Batchelor, G. K. (1967). *An Introduction to Fluid Dynamics*. Cambridge University Press, ISBN-13: 978-0521663960, ISBN-10: 0521663962, Cambridge.

Bonner, J. C.; Rice, A. B.; Lindroos, P. M.; O'Brien, P. O.; Dreher, K. L.; Rosas, I.; Alfaro-Moreno, E. & Osornio-Vargas, A. R. (1998). Induction of the lung myofibroblast PDGF receptor system by urban ambient particles from Mexico City. *Am. J. Respir. Cell. Molec. Biol.*, 19, 4, (October 1998) 672–680, ISSN: 1044-1549.

Bravo, H. A. & Torres, R. J. (2002). Air Pollution levels and trends in the Mexico City metropolitan area, In: *Urban Air Pollution and Forests: Resources at Risk in the Mexico City Air Basin,* M. Fenn, L. Bauer, and T. Hernández, (Eds.), 121–159, Springer-Verlag, ISBN:978-0-387-95337-3, New York.

Boghosian, B. M. (1999). Lattice Gases and Cellular Automata. *Future Generation Computer Systems*, 16, 2, (December 1999) 171-185(15). ISSN: 0167-739X.

Castro, T. & Salcido, A. (2006). Influencia de la Contaminación Atmosférica de la Zona Metropolitana de la Ciudad de México en Tres Sitios Perimetrales, In: *Contaminación Atmosférica V*, Leopoldo Garcia-Colin Scherer, Juan Ruben Varela Ham (Eds.), 119-144, El Colegio Nacional, ISBN: 970-640-303-5, Mexico.

Celada, A. T. & Salcido, A. (2009). The Mexico City 2006 Wind Direction States, *Proceedings of the 20th IASTED International Conference on Modelling and Simulation (MS 2009),* pp. 51-58, ISBN: 978-0-88986-799-4, Banff, Alberta, Canada, July 2009, Acta Press, Anaheim, Calgary, Zurich.

Chen, S.; Lee, M.; Zhao, K. H. & Doolen, G. D. (1989). A Lattice Gas Model with Temperature, *Physica D: Nonlinear Phenomena*, 37, 1-3, (July 1989) 42-59, ISSN: 0167-2789.

Chopard, B. & Droz, M. (1998). *Cellular Automata Modeling of Physical Systems*, CambridgeUniversity Press, ISBN-13: 9780521673457, Cambridge.

d´Humieres, D.; Lallemand, P. & Frish, U. (1986). Lattice Gas Models for 3D Hydrodynamics, *Europhys. Lett.*, 2, 4, (August 1986) 291-297, ISSN: 0295-5075.

Doran J. C.; Abbott S.; Archuleta J.; Bian X.; Chow J.; Coulter R. L.; Wekker S. F. J.; Edgerton S.; Elliott S.; Fernandez A.; Fast J. D.; Hubbe J.M.; King C.; Langley D.; Leach J.; Lee J.T.; Martin T.J.; Martinez D.; Martinez J.L.; Mercado G.; Mora V.; Mulhearn M.; Pena J.L.; Petty R.; Porch W.; Russell C.; Salas R.; Shannon J.D.; Shaw W.J.; Sosa G.; Tellier L.; Templeman B.; Watson J.G.; White R.; Whiteman C. & Wolfe, D. (1998). The IMADA-AVER boundary layer experiment in the Mexico City Area. *Bulletin of the American Meteorological Society,* 79, 11, (November 1998) 2497-2508, ISSN:1520-0477.

Doran J. C. & Zhong S. (2000). Thermally Driven Gap Winds into the Mexico City Basin, *Journal of Applied Meteorology,* 39, 8, (October 2000) 1330-1340, ISSN:08948763.

Frish, U.; Hasslacher, B. & Pomeau, Y. (1986). Lattice-Gas Automata for the Navier-Stokes Equation, *Phys. Rev. Lett.*, 56, 14, (April 1986) 1505-1508, ISSN: 1079-7114.

Garrat, J. R. (1992). *The Atmospheric Boundary Layer*, Cambridge University Press, ISBN:0-521-38052-9, Cambridge.

Hardy, J.; de Pazzis, O. & Pomeau, Y. (1976). Molecular Dynamics of a Classical Lattice Gas: Transport Properties and Time Correlation Functions, *Phys. Rev. A*, 13, 5, (May 1976) 1949-1961, ISSN: 1050-2947.

Hardy, J.; Pomeau, Y. & de Pazzis, O. (1973). Time Evolution of a Two-Dimensional Model System. I. Invariant States and Time Correlation Functions, *J. Math. Phys.* 14, 12, (December 1973) 1746-1759, ISSN: 0022-2488.

Hasslacher, B. (1987). Discrete Fluids, *Los Alamos Science*, 15, *Special Issue*, (1987) 175-217.

Jimenez, M. S.; Celada, A. T. & Salcido, A. (2008). The density of states of wind direction of the Mexico City Metropolitan Area: Year 2001, *Proceedings of the IASTED International Symposium on Environmental Modelling and Simulation (EMS 2008)*, pp. 301-307, ISBN: 978-0-88986-777-2, Orlando, USA, November 2008, Acta Press, Anaheim, Calgary, Zurich.

Kadanoff, L. P. & Swift, J. (1968). Transport Coefficients near the Critical Point: A Master-Equation Approach, *Phys. Rev.* 165, 1 (1968) 310-322, ISSN: 0031-899X.

MM5. (2003). MM5 Community Model. http://www.mmm.ucar.edu/mm5/mm5-home.html.

Osornio-Vargas, A. R.; Bonner, J. C.; Alfaro-Moreno, E.; Martinez, L.; Garcia-Cuellar, C.; Ponce-de-Leon-Rosales, S.; Miranda, J. & Rosas, I. (2003). Proinflammatory and cytotoxic effects of Mexico City air pollution particulate matter in vitro are dependent on particle size and composition. *Environ. Health Perspect.*, 111, 10, (August 2003) 1289–1293, ISSN: 0091-6765.

Rechtman, R.; Salcido, A. & Bagnoli, F. (1990). Thermomechanical Effects in a Nine-Velocities Two-Dimensional Lattice Gas Automaton, In: *Lectures on Thermodynamics and Statistical Mechanics,* M. López de Haro and C. Varea (Eds), 182-200, World Scientific., ISBN 981-02-0243-1, Singapore.

Rechtman, R.; Salcido, A. & Bagnoli, F. (1992). Some Near-Equilibrium Properties of a Nine-Velocities Lattice Gas Automaton for Two-Dimensional Hydrodynamics, In: *Complex Dynamics*, R. Livi, J-P. Nadal and N. Packard (Eds), 133-139, Nova Science Publishers Inc., ISBN: 1560720182, New York.

Rechtman, R. & Salcido, A. (1996). Lattice Gas Self Diffusion in Random Porous Media, *Fields lnstitute Communications,* 6 (1996) 217-225, ISSN: 1069-5265.

Rothman, D. & Zaleski, S. (1997). *Lattice-Gas Cellular Automata, Simple Models of Complex Hydrodynamics*, Cambridge University Press, ISBN: 0-521-55-201-X, Cambridge.

Salcido, A. & Rechtman, R. (1991). Equilibrium properties of a cellular automaton for thermofluid dynamics. In: *Nonlinear Phenomena in Fluids, Solids and Other Complex Systems*, P. Cordero and B. Nachtergaele (Eds), 217-229, Elsevier, ISBN: 0444887911, ISBN-13: 9780444887917, Amsterdam.

Salcido, A. & Rechtman, R. (1993). Lattice Gas Simulations of Flows Through Two-Dimensional Porous Media, *Proceedings of the International Symposium on Heat and Mass Transfer in Energy Systems and Environmental Effects*, pp. 222-226, Cancun, Mexico, August 1993, International Centre for Heat and Mass Transfer, Cancun.

Salcido, A. (1993). Lattice Gas Model for Transport and Dispersion Phenomena of Air Pollutants, In: *Transactions on Ecology and the Environment Vol. 1*, P. Zannetti, C.A. Brebbia, J.E. Garcia Gardea and G. Ayala Milian (Eds.), 173-181, WIT Press, ISSN: 1743-3541, Southamptom.

Salcido, A.; Merino, R. & Saldaña, R. (1993). Lattice Gas Model for Wind Fields over Complex Terrains. *Proceedings of the International Symposium on Heat and Mass Transfer in Energy Systems and Environmental Effects*, pp. 526-531, Cancun, Mexico, August 1993, International Centre for Heat and Mass Transfer, Cancun.

Salcido, A. (1994). First Evaluations of a Lattice Gas Approach to Air Pollution Modelling. In: *Transactions on Ecology and the Environment Vol. 3*, J. M. Baldasano, C. A. Brebbia, H. Power and P. Zannetti (Eds.), 141-150, WIT Press, ISSN 1743-3541, Southamptom.

Salcido, A.; Rodas, A.; Saldaña, R.; Miranda, U.; Sozzi, R. & Fraternali, D. (1994). Estudio de la Micrometeorología del Valle de México (Segunda Fase). Instituto de Investigaciones Eléctricas. Final Technical Report: IIE/15/0032/1 02/F (1994). Mexico.

Salcido, A; Celada, A. T.; Villegas, R.; Salas, H.; Sozzi, R. & Georgiadis, T. (2003a). A micrometeorological database for the Mexico City Metropolitan Area., *Il Nuovo Cimento*, 26C, 3, (May/June 2003) 317-355, ISSN: 11241896.

Salcido, A.; Sozzi, R. & Castro, T. (2003b). A Least Squares Variational Approach to the Convective Mixing Height Estimation Problem. *Environmental Modelling & Software*, 18, 10, (December 2003) 951-957, ISSN: 13648152.

Salcido, A.; Celada-Murillo, A. T. & Castro, T. (2008). Lattice Gas Simulation of Wind Fields in the Mexico City Metropolitan Area, *Proceedings of the 19th IASTED International Conference on Modelling and Simulation (MS 2008),* pp. 95-100, ISBN: 9780889867413, Quebec, Canada, May 2008, Acta Press, Anaheim, Calgary, Zurich.

Sciarretta, A. & Cipollone, R. (2001). A lattice gas model for the evaluation of transport and diffusion parameters of stack emissions in air. In: *Air Pollution IX*, G. Latini and C. A. Brebbia (Eds), WIT Press, ISBN: 1853128775, Southampton.

Sciarretta, A. & Cipollone, R. (2002). On the evaluation of pollutant gas dispersion around complex sources by means of a lattice gas model. In: *Air Pollution X*, C. A. Brebbia and J. Martin-Duque (Eds), pp. 33-42, WIT Press, ISBN: 185312916X, Southampton.

Sciarretta, A. (2006). A lattice gas model with temperature and buoyancy effects to predict the concentration of pollutant gas released by power plants and traffic sources, *Mathematical and Computer Modelling of Dynamical Systems*, 12, 4, (August 2006) 313-327, ISSN: 1387-3954.

SMA-GDF. (2006). *Informe Climatológico Ambiental del Valle de México 2006.* Secretaria del Medio Ambiente del Gobierno del Distrito Federal. México.

SMA-GDF. (2008). *Inventario de Emisiones de Contaminantes Criterio de la Zona Metropolitana del Valle de México 2006*. Secretaría del Medio Ambiente. Gobierno del Distrito Federal. México.

Toffoli, T. (1984). Cellular automata as an alternative to (rather than an approximation of) differential equations in modeling physics, *Physica D*, 10, 1, (January 1984) 117-127, ISSN: 0167-2789.

UNEP (United Nations Environment Programme) & WHO (World Health Organization). (1992). *Urban Air Pollution in Megacities of the World,* Blackwell Publishers, Oxford.

Von Neumann, J. (1966). The *Theory of Self-Reproducing Automata,* University of Illinois Press, ISBN: 0598377980, Urbana.

Wolfram, S. (1986). Cellular Automaton Fluids I. Basic Theory, *J. Stat. Phys.* 45, 3-4, (November 1986) 471-526, ISSN: 00224715.

Zannetti, P. (1990). *Air Pollution Modelling. Theories, Computational Methods and Available Software*, Computational Mechanics Publications, ISBN: 0442308051, Southampton, Boston, New York.

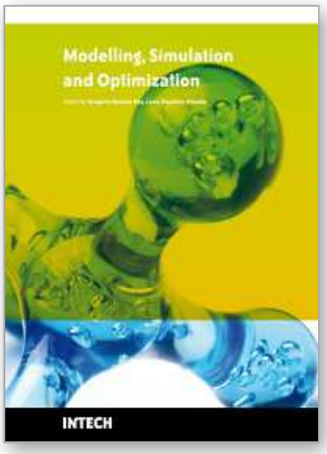

Modelling Simulation and Optimization

Edited by Gregorio Romero Rey and Luisa Martinez Muneta

ISBN 978-953-307-048-3
Hard cover, 708 pages
Publisher InTech
Published online 01, February, 2010
Published in print edition February, 2010

Computer-Aided Design and system analysis aim to find mathematical models that allow emulating the behaviour of components and facilities. The high competitiveness in industry, the little time available for product development and the high cost in terms of time and money of producing the initial prototypes means that the computer-aided design and analysis of products are taking on major importance. On the other hand, in most areas of engineering the components of a system are interconnected and belong to different domains of physics (mechanics, electrics, hydraulics, thermal...). When developing a complete multidisciplinary system, it needs to integrate a design procedure to ensure that it will be successfully achieved. Engineering systems require an analysis of their dynamic behaviour (evolution over time or path of their different variables). The purpose of modelling and simulating dynamic systems is to generate a set of algebraic and differential equations or a mathematical model. In order to perform rapid product optimisation iterations, the models must be formulated and evaluated in the most efficient way. Automated environments contribute to this. One of the pioneers of simulation technology in medicine defines simulation as a technique, not a technology, that replaces real experiences with guided experiences reproducing important aspects of the real world in a fully interactive fashion [iii]. In the following chapters the reader will be introduced to the world of simulation in topics of current interest such as medicine, military purposes and their use in industry for diverse applications that range from the use of networks to combining thermal, chemical or electrical aspects, among others. We hope that after reading the different sections of this book we will have succeeded in bringing across what the scientific community is doing in the field of simulation and that it will be to your interest and liking. Lastly, we would like to thank all the authors for their excellent contributions in the different areas of simulation.

InTech Europe
University Campus STeP Ri
Slavka Krautzeka 83/A

InTech China
Unit 405, Office Block, Hotel Equatorial Shanghai
No.65, Yan An Road (West), Shanghai, 200040, China

51000 Rijeka, Croatia
Phone: +385 (51) 770 447
Fax: +385 (51) 686 166
www.intechopen.com

中国上海市延安西路65号上海国际贵都大饭店办公楼405单元
Phone: +86-21-62489820
Fax: +86-21-62489821

IntechOpen

IntechOpen